dimensional pore structure of SBA-1, which limits pore blocking and allows a faster diffusion of the reactant molecules.

In conclusion, our results reveal that Fe has been successfully incorporated, for the first time, into SBA-1 by simply adjusting the molar hydrochloric acid to surfactant ratio. UV-vis DRS and ESR studies confirm that the majority of the Fe atoms in FeSBA-1 exist in a tetrahedral coordination environment (most probably occupying framework positions). The catalytic activity of the novel catalyst was investigated in the vapor phase *tert*-butylation of phenol reaction. FeSBA-1(36) was found to be more active than previously studied systems such as FeAlMCM-41 or sulfated zirconica. The observed phenol conversion of 78.8 % ($S_{4\text{-TBP}} = 70$ %) is significantly higher as compared to other mono- and bimetal substituted uni-dimensional MCM-41 molecular sieves under optimized reaction conditions.[13,17]

Experimental

Iron containing SBA-1 was synthesized under acidic conditions using cetyltriethylammonium bromide (CTEABr) as the surfactant, tetraethylorthosilicate (TEOS) as the silica source and ferric nitrate nonahydrate as the iron source. The surfactant (CTEABr) was synthesized by the reaction of 1-bromohexadecane with an equimolar amount of triethylamine in ethanol under reflux conditions for two days. The resulting solid CTEABr was purified via recrystallization from a chloroform/ethyl acetate mixture. A typical synthesis procedure for FeSBA-1 is as follows: Solution A was prepared by adding 0.812 g of CTEABr to an appropriate amount of the aqueous solution of 4.4 M HCl (n_{HCl}/n_{H_2O} ratio was fixed to 0.08). The solution thus obtained was cooled to 0 °C and homogenized for 30 min. TEOS and $Fe(NO_3)_3 \cdot 9H_2O$ were precooled to 0 °C and then added to solution A under vigorous stirring and continued the stirring for another 5 h at 0 °C. Thereafter, the reaction mixture was heated to 100 °C for 1 h. The samples were labeled FeSBA-1(x) where x denotes the n_{Si}/n_{Fe} molar ratio. The solid product was recovered by filtration and dried in an oven at 100 °C overnight. The molar composition of the gel was 1 TEOS:0.0025–0.025 Fe_2O_3:0.2 CTEABr:10–56 HCl:125–700 H_2O. The as-synthesized material was then calcined in air by raising the temperature from 20 to 550 °C with a heating rate of 1.8 °Cmin^{-1} and keeping the sample at the final temperature for 10 h.

Received: February 18, 2004
Final version: May 28, 2004

[1] H.-Y. Chen, W. M. H. Sachtler, *Catal. Today* **1998**, *42*, 73.
[2] A. E. Shilov, G. B. Shulpin, *Chem. Rev.* **1997**, *97*, 2879.
[3] J. Valyon, W. S. Millman, W. K. Hall, *Catal. Lett.* **1994**, *24*, 215.
[4] C. T. Kresge, M. E. Leonowicz, W. J. Roth, J. C. Vartuli, J. S. Beck, *Nature* **1992**, *359*, 710.
[5] S. Che, A. E. G. Bennet, Y. Yokoi, K. Sakamoto, H. Kunieda, O. Terasaki, T. Tatsumi, *Nat. Mater.* **2003**, *2*, 801.
[6] D. Zhao, Q. Huo, J. Feng, B. F. Chmelka, G. D. Stucky, *J. Am. Chem. Soc.* **1998**, *120*, 6024.
[7] Q. Zhang, K. Ariga, A. Okabe, T. Aida, *J. Am. Chem. Soc.* **2004**, *126*, 988.
[8] Q. Huo, R. Leon, P. M. Petroff, G. D. Stucky, *Science* **1995**, *268*, 1324.
[9] M. J. Kim, R. Ryoo, *Chem. Mater.* **1999**, *11*, 487.
[10] A. Vinu, V. Murugesan, M. Hartmann, *Chem. Mater.* **2003**, *15*, 1385.
[11] a) L.-X. Dai, K. Tabata, E. Suzuki, T. Tatsumi, *Chem. Mater.* **2001**, *13*, 208. b) L.-X. Dai, Y.-H. Teng, K. Tabata, E. Suzuki, T. Tatsumi, *Chem. Lett.* **2000**, 794.
[12] a) A. Sakthivel, S. K. Badamali, P. Selvam, *Microporous Mesoporous Mater.* **2000**, *39*, 457. b) S. K. Badamali, A. Sakthivel, P. Selvam, *Catal. Lett.* **2000**, *65*, 153. c) A. Sakthivel, N. Saritha, P. Selvam, *Catal. Lett.* **2001**, *72*, 225.
[13] S. Bordiga, R. Buzzoni, F. Geobalda, C. Lamberti, E. Giomello, A. Zecchina, G. Leofani, G. Petrini, G. Tozzola, G. Vlaic, *J. Catal.* **1996**, *158*, 486.
[14] Y. Wang, Q. Zhang, T. Shishido, K. Takehira, *J. Catal.* **2002**, *209*, 186.
[15] A. Tuel, I. Acron, J. M. M. Millet, *J. Chem. Soc. Faraday Trans.* **1998**, *94*, 3501.
[16] a) D. Goldfarb, M. Bernardo, K. G. Strohmaier, D. E. W. Vaughan, H. Thomann, *J. Am. Chem. Soc.* **1994**, *116*, 6344. b) D. Goldfarb, K. G. Strohmaier, D. E. W. Vaughan, H. Thomann, O. G. Poluetkov, J. Schmidt, *J. Am. Chem. Soc.* **1996**, *118*, 4665.
[17] A. Vinu, K. Usha Nandhini, V. Murugesan, W. Böhlmann, V. Umamaheswari, A. Pöppl, M. Hartmann, *Appl. Catal. A* **2004**, *265*, 1.
[18] K. Zhang, C. Huang, H. Zhang, S. Xiang, S. Liu, D. Xu, H. Li, *Appl. Catal. A* **1998**, *166*, 89.
[19] R. C. Deka, R. Vetrivel, *J. Catal.* **1998**, *174,* 88.
[20] K. Zhang, C. Huang, H. Zhang, S. Xiang, S. Liu, D. Xu, H. Li, *Appl. Catal. A* **1998**, *166*, 89.
[21] C. Song, X. Ma, A. D. Schmitz, H. H. Schobert, *Appl. Catal. A* **1999**, *182*, 175.

Enhancing the Rate of Energy Release from NanoEnergetic Materials by Electrostatically Enhanced Assembly**

By *Soo H. Kim* and *Michael R. Zachariah**

Energetic materials are classified as those that convert chemical enthalpy to thermal enthalpy rapidly. They are commonly used in explosives, propulsion, and pyrotechnics. The synthesis of nanostructured energetic materials has recently drawn considerable attention as a potential method that can be used to obtain energy release more rapidly than conventional materials. It is known that the size distribution and the degree of intermixing of thermite-like reactants (e.g., metal/metal oxide) significantly affects the burning rate of energetic materials. For instance, nanoparticles of fuel/oxidizer materials have been reported to have burning rates ~1000 times higher. This is presumably due to the reduction of the diffusion distance between ultrafine grain (UFG) intermixed reactants.[1]

[*] Prof. M. R. Zachariah, Dr. S. H. Kim
Center for NanoEnergetics Research
Departments of Mechanical Engineering and Chemistry
University of Maryland and
the National Institute of Standards and Technology
Gaithersburg, MD 20899-8360 (USA)
E-mail: mrz@umd.edu

[**] Partial support for this work comes from the US Army–DURINT Center for NanoEnergetics Research and the National Institute of Standards and Technology.

DOI: 10.1002/adma.200306436

ADVANCED MATERIALS

Generally, fuel and oxidizer powder are physically mixed to produce an energetic mixture that can undergo a thermite reaction.

$$M^1_{(s)}+M^2O_{(s)} \rightarrow M^1O_{(s)}+M^2_{(s)}+\Delta H \quad (1)$$

where for example, M^1 (fuel metal particle) is Al undergoing rapid exothermic reaction with M^2O (oxidizer particles such as Fe_2O_3, MoO_3, or CuO). Once initiated, such reactions are self-sustaining, however, the reactants must still physically mix, and therefore the mass transfer process may ultimately be the rate limiting step, retarding the rate of energy release. Recent work has focused on making the fuel and oxidizer grains physically smaller, entering the nanometer scale so as to minimize mass transfer effects.[2] In this latter example, researchers at Lawrence Livermore National Laboratories (LLNL) devised a sol–gel approach in order to manufacture thermite composites.

In a related study, we extended the LLNL work, by adapting the sol–gel beaker chemistry to develop an aero-sol–gel method. This negated the need to grind the product into powder. We were successful in developing an aerosol route to produce nanoporous metal oxide particles and in particular for energetic applications of iron oxide (Fe_2O_3).[3,4] However, in those studies, the intermixing of reactant particles required a secondary step of ultrasonic mixing and subsequent drying. Furthermore this approach relies on a random mixing process, rather than a directed assembly between fuel and oxidizer.

In this paper, we demonstrate a new method for the synthesis of nanostructured fuel/metal oxidizer nanocomposites in which the fuel and oxidizer association is enhanced by the electrostatic forces which exist between charged aerosol particles. Our goal is to enhance the interaction of fuel and oxidizer and minimize fuel–fuel and oxy–oxy interactions by oppositely charging each component aerosol. The specific example in this paper involves an aluminum/iron oxide thermite mixture and we will show that such an approach leads to a significantly higher energy release rate.

The nanoscale assembly of the reactant particles in this approach is strongly dependent on the collision rate between fuel and metal oxidizer nanoparticles. To verify the effect of charge on the particle collision rate, the characteristic collision time, t, between particles carrying charges of opposite sign is calculated as a function of particle number concentration, and degree of particle charge with fixed particle sizes at room temperature.[5]

$$t = \frac{2}{K_{ij}^{p,q} \cdot N_p} \quad (2)$$

where, $K_{ij}^{p,q} = K_{ij}/W_{ij}^{p,q}$, K_{ij} is the coagulation coefficient of neutral particles, $W_{ij}^{p,q}$ is the Fuchs stability function $(= {}^1/_Z(\exp\ (z)-1))$ where $Z = 2pqe^2/(d_{pi}+d_{qj})K_BT$, p, q are the number of elementary charges on particles, e is the elementary unit of charge, d_{pi}, d_{qj} is the particle diameter, K_B is the Boltzmann constant, and T is the gas temperature.

Obviously, and as can be seen in Equation 2, oppositely charged particles aggregate faster than particles with same sign. Furthermore, an increase in the initial number concentration of particles shortens the collision time between particles, and while this is desirable, we were ultimately limited by the nature of our atomization process. We were however able to vary the extent of charging over a relatively wide range.

Figure 1 summarizes the experimentally determined relative characteristic times for oppositely charged particle collisions, normalized to Brownian collisions as a function of degree of particle charge. By varying the applied voltage in the corona charger, various charge levels on particles were experimentally obtained, from 5 charges/particle with concentrations of $\sim 10^7$ cm^{-3} to a maximum of 30 charges/particle with concentrations $\sim 10^6$ cm^{-3}. For these measurements the average particle charge ($\bar{n}_p$) was determined by,

$$\bar{n}_p = \frac{I}{N_{total} e Q} \quad (3)$$

where I is the induced current at the electrometer, N_{total} is the total number concentration of particles determined by the condensation nucleus counter (CNC), and Q is the aerosol flow rate. The high particle charge limit of ~30 charges/particle was a compromise. Namely, the number concentration of particles that penetrated the unipolar charger at high applied voltage was significantly reduced due to the electrostatic deposition at the charger nozzle and ultimately results in an increase in characteristic collision time and very low yield. Over the range of experiments reported here however, despite particle loss, we observed a decrease in the characteristic collision time with an increase in the extent of charging.

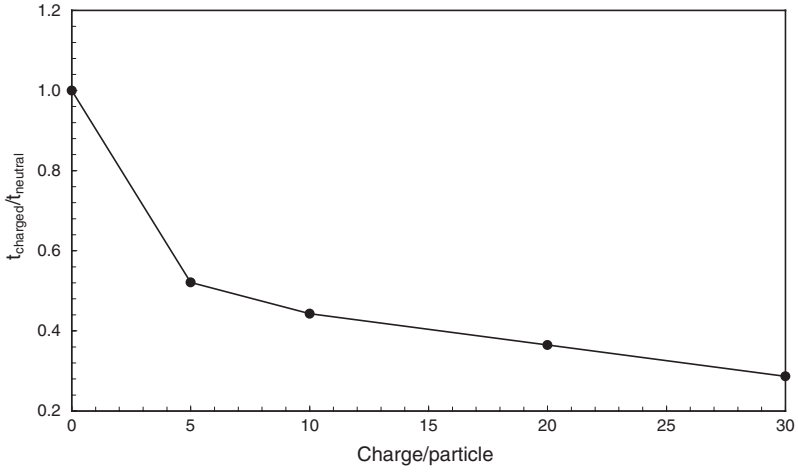

Figure 1. Relative characteristic collision time of 200 nm-diameter average particles as a function of number of elementary charges measured. $K_{ij} = 5.2 \times 10^{-10}$ cm^3 s^{-1} for these experimental conditions.

The size distribution of reactant particles and their electrostatically enhanced collision was measured with a differential mobility particle sizer (DMPS)[6] (summarized in Fig. 2). The geometric mean diameter (GMD) of aluminum and iron oxide particles were found to be 150 and 200 nm, respectively. Allowing for the interaction of the two aerosol streams gave a GMD of 215 nm for Brownian coagulation and 225 nm for bipolar coagulation with a similar polydispersity (geometric standard deviation ~1.37). Apparently, both Brownian and bipolar coagulation events caused approximately the same decrease in particle number concentration and increase of particle size. However, these results mask the fact that under charge conditions, electrostatic loss results in a significant reduction of the effect of bipolar coagulation between the reacting particles. Nevertheless, the action of charge should be to enhance the collisions between particles of opposite charge and simultaneously decrease like charge interactions.

The particles produced by Brownian and bipolar coagulation processes were observed under transmission electron microscopy (TEM) to identify the effect of particle charge on morphology of the nanocomposite particle and were verified by scanning transmission microscopy (STEM) elemental mapping. In the Brownian collision case (see Fig. 3a), aluminum nanoparticles appear to have linear chains that are held together by weak contact with the iron oxide particles. However, for bipolar coagulation as shown in Figure 3b, the aluminum nanoparticles essentially surround the surface of iron oxide particles. Because of the nature of the aero-sol–gel chemistry, whereby the iron-oxide begins as a droplet we observe in some cases that the aluminum can penetrate within the iron-oxide gel. This is consistent with our conceptual model (suggested in Figure 4), which illustrates which charge enhanced collisions will lead to a greater pairing and intimate contact between fuel and oxidizer.

To evaluate qualitatively the effect of particle charging on reactivity, a 15 mg sample was spark ignited at one end. Figure 5a, shows a snapshot of the burning sample prepared via Brownian assembly. The sample was observed to burn nonhomogeneously. We observed that as we increased the degree of particle charge, the velocity of propagating flame as it traversed from one end of the sample to the other was significantly enhanced. Figure 5b illustrates the case of a sample that was generated with 30 charges/particle, which produced a bright flash and a propagation velocity so fast as to be essentially instantaneous to the naked eye. This simple demonstration is convincing proof that electrostatically enhanced fuel/oxidizer assembly greatly enhances the mixing of fuel and oxidizer at the nanoscale level.

To further quantify this effect, differential scanning calorimetry (DSC) analysis was performed on both the randomly assembled (Brownian) and electrostatically assembled nanocomposite and are shown in Figure 6. Quite clearly both show an exotherm, and both show essentially a similar ignition temperature as one might expect. The DSC shows that the rate of exotherm observed in the electrostatically enhanced case is a factor of 10 faster. Inte-

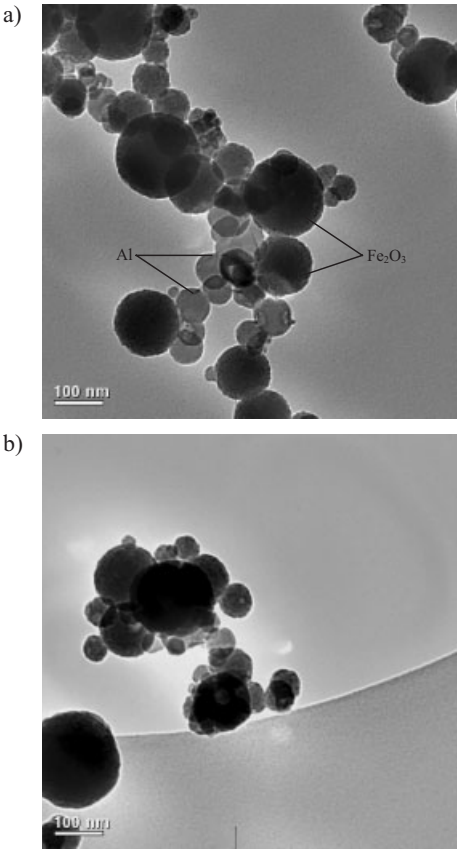

Figure 3. TEM images of nanocomposite particles produced by a) Brownian coagulation and b) bipolar coagulation. Elemental composition was verified by STEM elemental mapping.

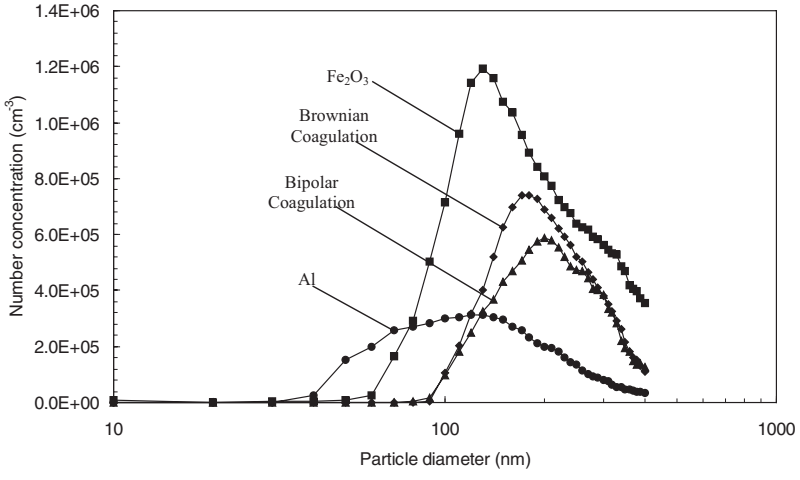

Figure 2. Particle size distribution of aerosolized UFG aluminum and iron oxide particles: effect of Brownian and bipolar coagulation on the final nanocomposite particle size distribution.

ADVANCED MATERIALS

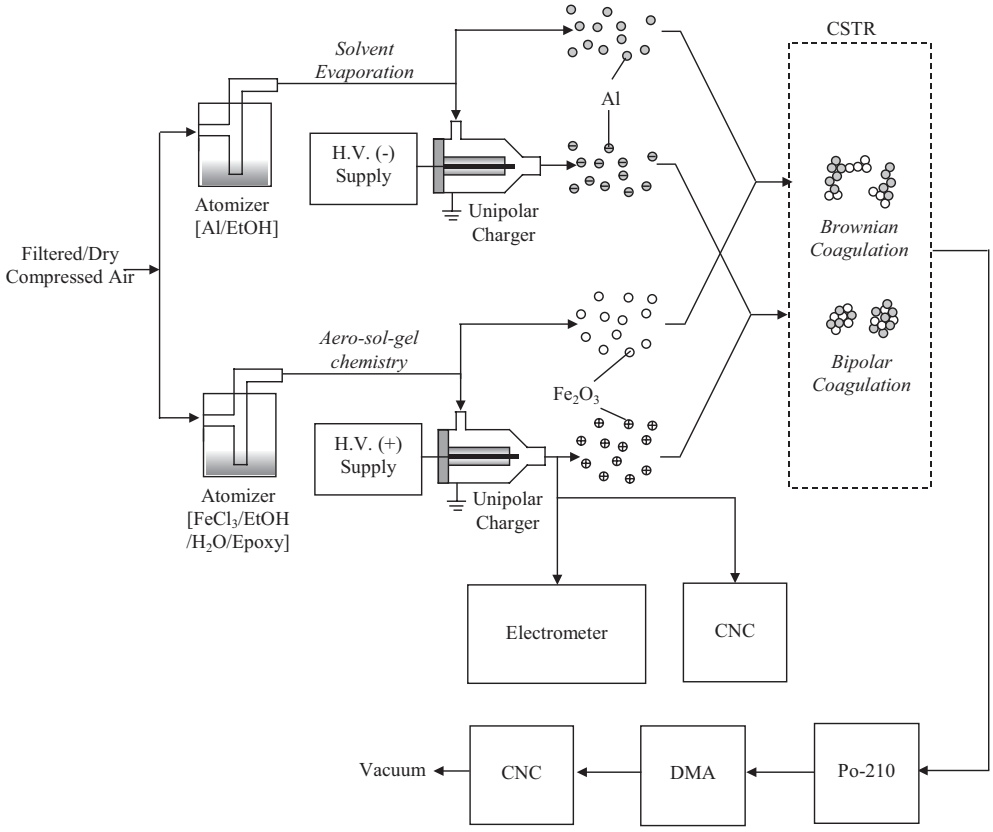

Figure 4. Schematic of the experiment. In-situ particle size distribution (PSD) measurement is made using a differential mobility particle sizer, composed of a radioactive ionizing source, differential mobility analyzer (DMA), and condensation nucleus counter (CNC). The electrometer combined with the CNC is employed to measure the average charge of particles generated from the unipolar charger.

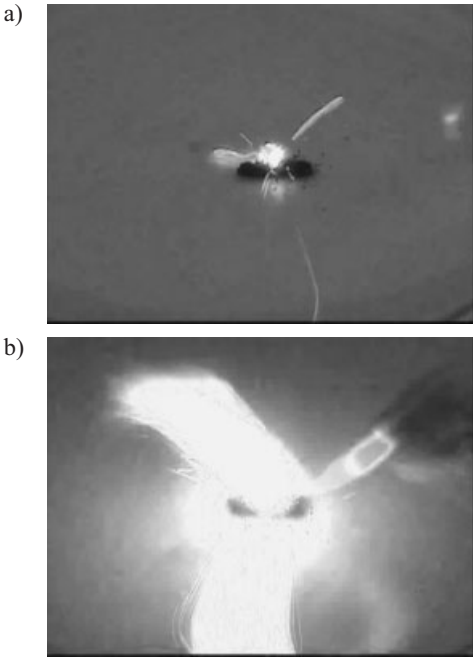

Figure 5. Photograph of thermally ignited aluminum and iron oxide nanocomposite for particles produced by a) Brownian coagulation and b) bipolar coagulation (30 charges/particle).

gration of the exotherm gives a total heat of reaction of 0.7 kJ g^{-1} over a relatively wide temperature range for the Brownian assembled particles (Fig. 6a), but a total heat of 1.8 kJ g^{-1} over a very narrow temperature range was observed for the electrostatically assembled case (Fig. 6b). However, both experimentally determined values of total heat of reaction are lower than the theoretical value of 3.9 kJ g^{-1}. We believe this short fall is likely due to 1) an oxide layer on the aluminum particles, and 2) incomplete conversion in the sol–gel chemistry to form iron oxide. STEM elemental mapping did show that residual chlorine from the precursor iron chloride remained in the sample. Nevertheless, it is quite clear that for the same starting reactant particles, electrostatically assembled nanocomposites resulted in a significantly enhanced energy release rate and total extent of reaction.

In conclusion, we have demonstrated the potential of electrostatically enhanced nanocomposite particle assembly as a viable method that can be used to enhance the reactivity of energetic nanocomposites. We have shown that one can tailor the kinetics of the burning process by varying the degree of interconnection between the reactant nanoparticles by varying the magnitude of particle charge. The results of burning tests and thermal analysis using differential scanning calorimetry (DSC), showed that aluminum/iron oxide nanocomposite aerosol materials synthesized via bipolar assembly had burn-

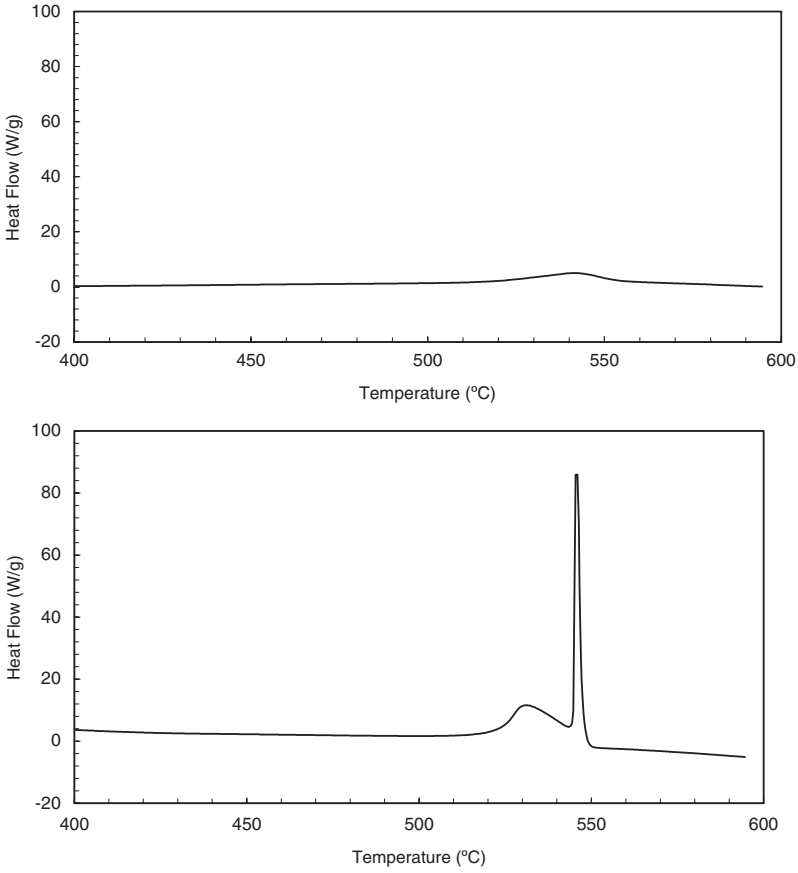

Figure 6. DSC results of Al/Fe_2O_3 nanocomposite particles, produced by a) Brownian coagulation and b) bipolar coagulation (30 charges/particle).

ing rates that were a factor of ten higher than those produced by random Brownian coagulation. By employing the aerosol synthetic route, one may be able to rapidly and reproducibly obtain nanocomposite energetic materials with high purity and controlled fuel and oxidizer balances.

Experimental

The fuel used for this work was commercially available (NanoTech Inc.) passivated aluminum nanopowder with average primary particle size ~ 50 nm. The nanoporous iron oxide particles were created in situ using a procedure outlined in our prior work [4]. Iron(III) chloride ($FeCl_3 \cdot 6H_2O$) and epoxide (1,2-epoxy butane) were the precursors used for the iron oxide. To make a stoichiometric mixture of nanocomposite particles, two atomizers with controlled amounts of precursors were prepared in ethanol (EtOH). In one atomizer we dispersed 0.38 g of aluminum nanopowder into 40 mL of ETOH; in the other, 1.25 g of iron(III) chloride, 5 mL of epoxide, and 1 mL of H_2O was dissolved into 40 mL of EtOH.

Two Collision atomizers were employed as shown in Figure 4. Aerosol from the first atomizer containing the aluminum nanoparticles dispersed in ethanol was stripped of the solvent by passing through a diffusion dryer containing silica gel and activated charcoal. The second atomizer generated the droplets of iron chloride, epoxide, and water, which underwent a sol–gel reaction in the droplet to form iron oxide (Fe_2O_3) via our aero-sol–gel approach described elsewhere [4].

The aerosol particles were then charged by diffusion charging of gas ions generated from homebuilt unipolar corona chargers operating at up to ~ 4 kV, and constructed of a high voltage-connected cylindrical tungsten electrode (outer diameter 1 mm) and a grounded aluminum housing with tapered outlet [7]. To assess the extent of charging as a function of applied voltage, the average charge on particles was measured with an aerosol electrometer (TSI, Model 3068A) and total concentration with a condensation nucleus counter (TSI, Model 3022). The individual oppositely charged particle streams were then mixed in the continuous stirring tank reactor (CSTR) with total volume of 56.8 L. The particle residence time was about 10 min, aerosol flow rate from each atomizer was 3 L m^{-1}. The final composite particles were collected on either a membrane filter (Millipore co.) or TEM grid for thermal analysis and morphology characterization of the nanocomposite.

The nanocomposite particles were characterized with a transmission electron microscope, (TEM; JEOL 1210) operated at 100 kV,a scanning transmission electron microscope (STEM; Philips CM30) operated at 300 kV, energy dispersive spectrometry (EDS; EDAX PV9900), and differential scanning calorimetry (DSC; Perkin-Elmer Pyris-1) operated at temperatures ranging from 25 to 600 °C (heating rate, 10 °C min^{-1}) with 5 mg of sample.

Received: November 7, 2003
Final version: January 26, 2004
Published online: September 23, 2004

[1] W. C. Danen, J. A. Martin, *US Patent No. 5 266 132*, **1993**.
[2] T. M. Tillotson, A. E. Gash, R. L. Simpson, L. W. Hrubesh, J. H. Satcher, Jr., J. F. Poco, *J. Non-Cryst. Solids* **2001**, *285*, 338.
[3] S. H. Kim, B. Y. H. Liu, M. R. Zachariah, *Langmuir* **2004**, *20*, 2523.
[4] A. Prakash, A. V. McCormick, M. R. Zachariah, *Chem. Mater.* **2004**, *16*, 1466.
[5] J. H. Seinfeld, S. N. Pandis, *Atmospheric Chemistry and Physics*, John Wiley & Sons, New York **1998**.
[6] H. Fissan, C. Helsper, H. J. Thielen, *J. Aerosol Sci.* **1983**, *14*, 354.
[7] A. Hernandez-Sierra, F. J. Alguacil, M. Alonso, *J. Aerosol Sci.* **2003**, *34*, 733.

